Supporting Information

One-Stone-Two-Birds: High-Density Single-Site Cobalt in Hierarchical Zeolite Boosts Aerobic Styrene Epoxidation

Chun-Mu Guo[a], Zhan Liu[a], An-Kang Jiang[a], Ming-Hui Sun[a], Bo Ye[a], Jia-Min Lyu[a], Ke Min[a], Xiao-Yu Yang[a], Ke Lyu[a], Xiao-Yun Li[b], Yu Li[a], Li-Hua Chen[a]*, Bao-Lian Su[a,c]*

a State Key Laboratory of Advanced Technology for Materials Synthesis and Processing, Wuhan University of Technology, Wuhan, Hubei 430070, China.

b State Key Laboratory of Silicate Materials for Architectures, Wuhan University of Technology, Wuhan, Hubei 430070, China.

c Laboratory of Inorganic Materials Chemistry (CMI) University of Namur 61 rue de Bruxelles Namur 5000, Belgium.

** Corresponding author:*

Prof. Ming-Hui Sun (sunminghui@whut.edu.cn)

Prof. Li-Hua Chen (chenlihua@whut.edu.cn).

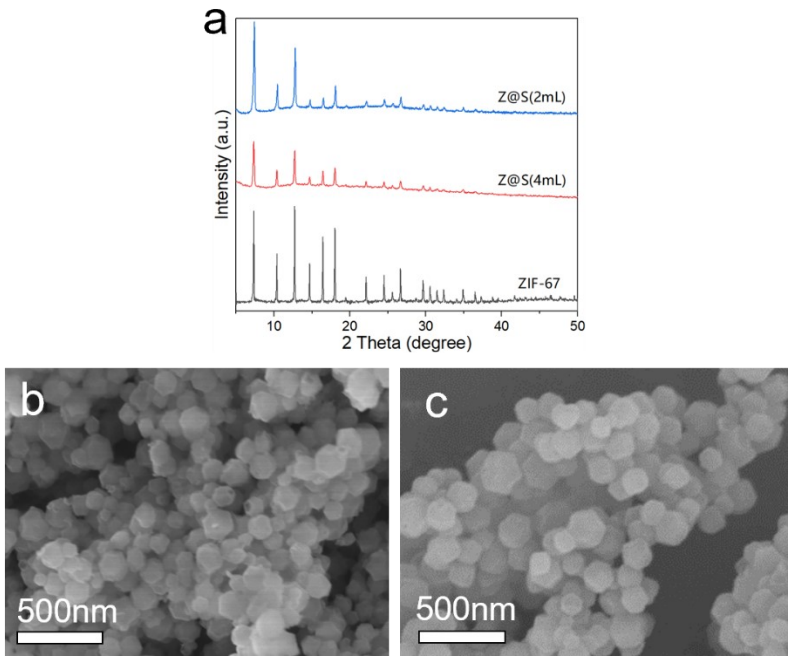

Fig. S1 (a) XRD patterns of ZIF-67, Z@S(2mL) and Z@S(4mL); SEM images of (b) Z@S(2mL) and (c) Z@S(4mL).

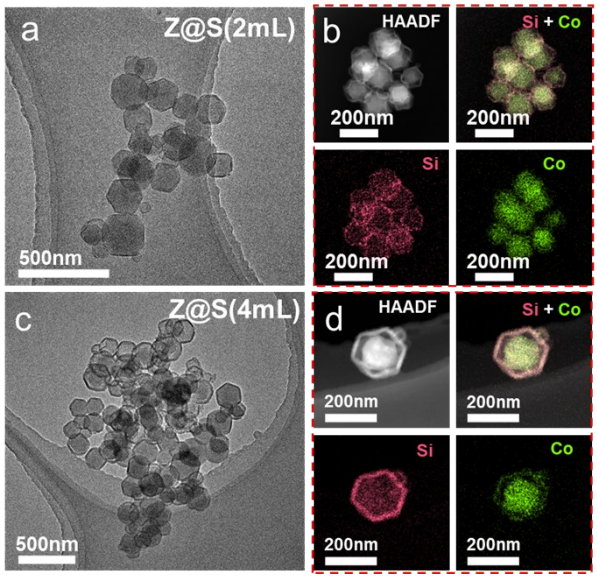

Fig. S2 TEM images of (a) Z@S(2mL) and (c) Z@S(4mL); (b) HAADF and elemental mapping images of Z@S(2mL) and (d) Z@S(4mL).

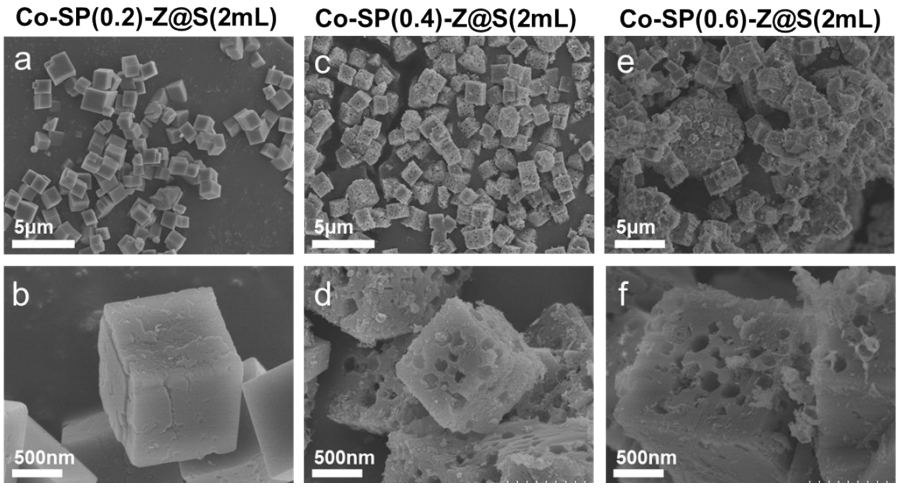

Fig. S3 SEM images of (a, b) Co-SP(0.2)-Z@S(2mL); (c, d) Co-SP(0.4)-Z@S(2mL) and (e, f) Co-SP(0.6)-Z@S(2mL).

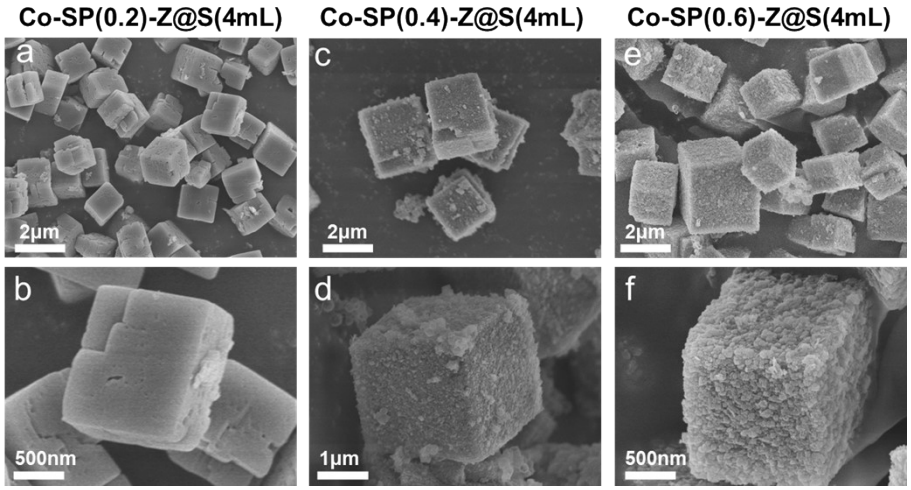

Fig. S4 SEM images of (a, b) Co-SP(0.2)-Z@S(4mL); (c, d) Co-SP(0.4)-Z@S(4mL) and (e, f) Co-SP(0.6)-Z@S(4mL).

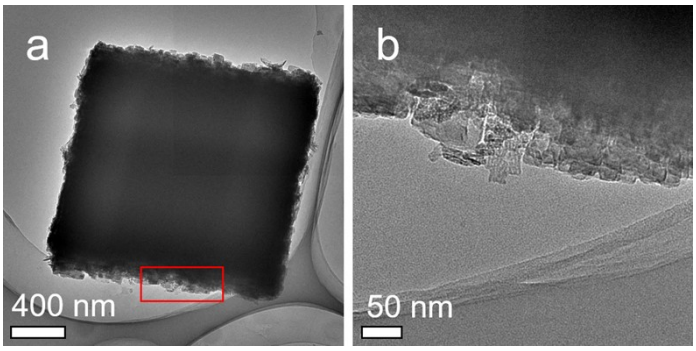

Fig. S5 TEM image of the Co-SP(0.6)-Z@S(4mL) sample.

Note: No distinct mesoporous or macroporous structures are observed within the interior of the Co-SP(0.6)-Z@S(4mL) crystals. Instead, an accumulation of small nanocrystals is observed on the external surface, which is consistent with the SEM observations. The inter-crystalline mesopores formed by the aggregation of these small grains account for the slight increase in the external surface area and mesopore volume of the sample.

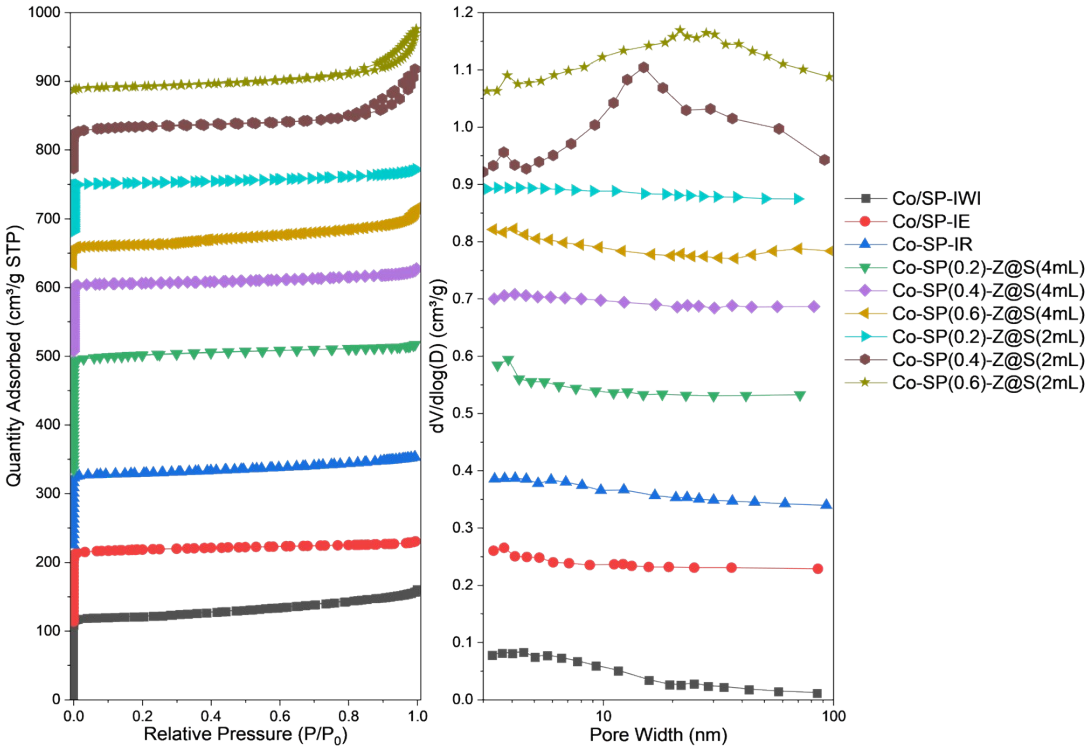

Fig. S6 N_2 adsorption-desorption isotherms of the samples.

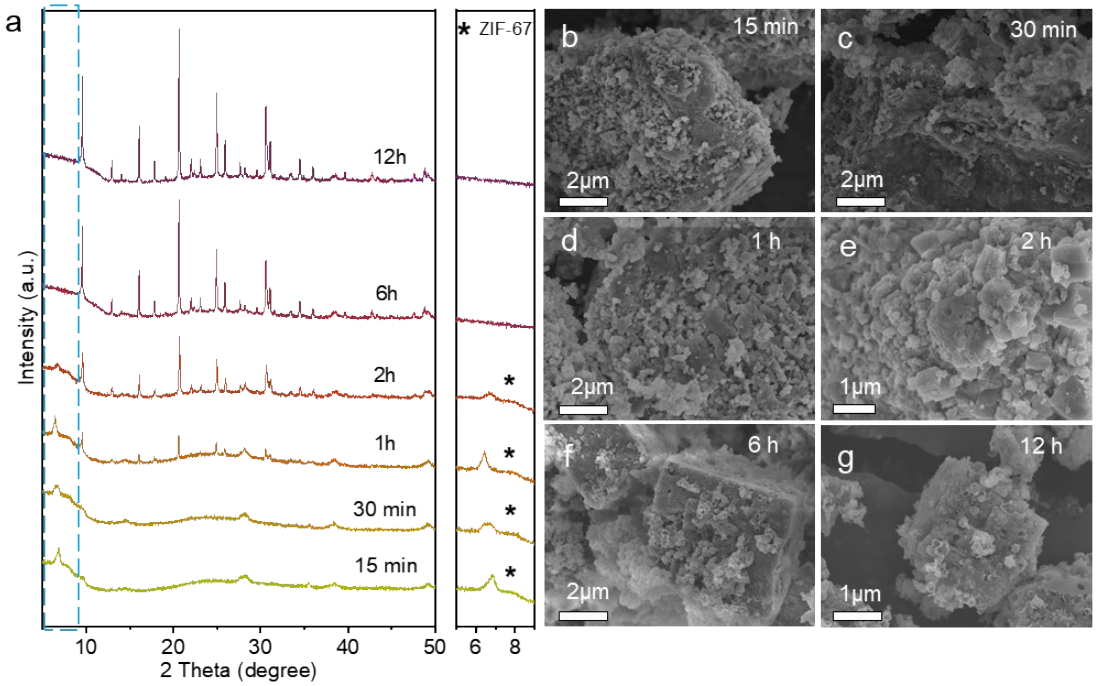

Fig. S7 (a) XRD patterns of Co-SP(0.4)-Z@S(2mL) crystallized for different durations and (b–g) the corresponding SEM images.

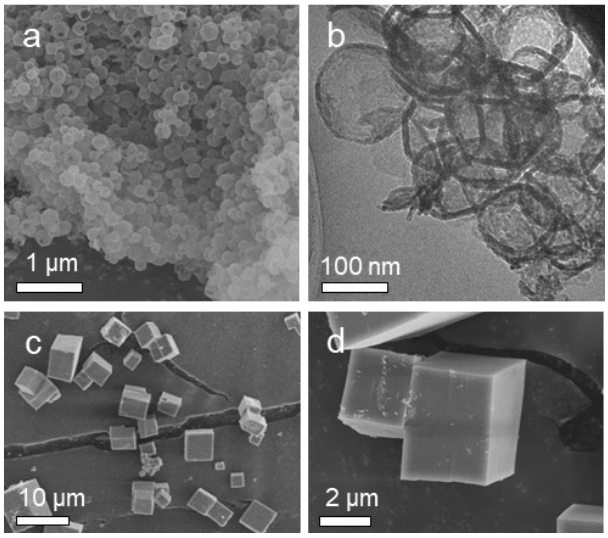

Fig. S8 (a) SEM and (b) TEM images of hollow SiO_2; (c–d) SEM images of SP(0.4)-$HSiO_2$ synthesized with hollow SiO_2 as the silica source.

Note: Hollow SiO_2: Prepared by stirring the ZIF-67@SiO_2 (2 mL TEOS) precursor in a dilute HCl solution (0.1M) for 1 h, followed by washing and drying.

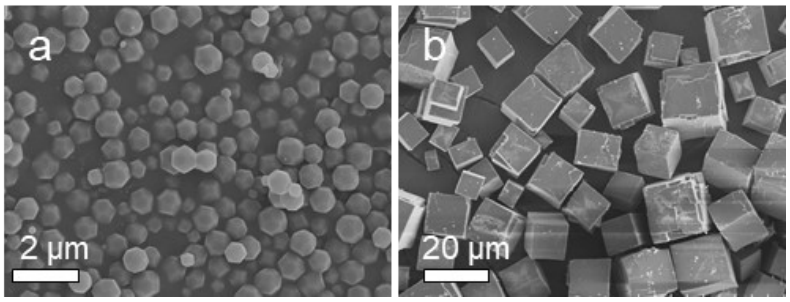

Fig. S9 (a) SEM image of bare ZIF-67 (without SiO_2 shell) and (b) SEM image of Co-SP(0.4)-Z obtained therefrom.

Note：Pristine ZIF-67: Synthesized using the same procedure as ZIF-67@SiO_2 but without the addition of TEOS

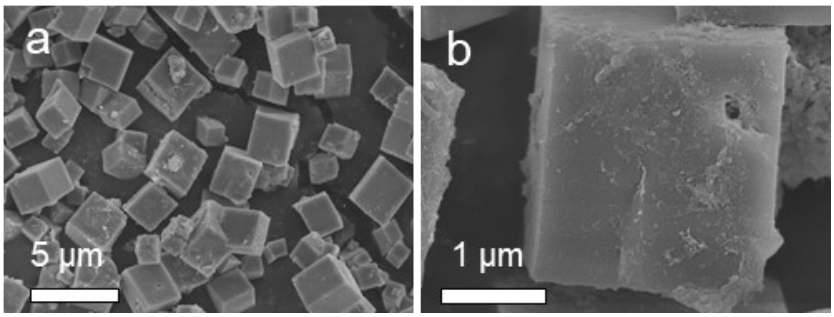

Fig. S10 SEM images of the Co-SP(0.4)-Z-$HSiO_2$ sample.

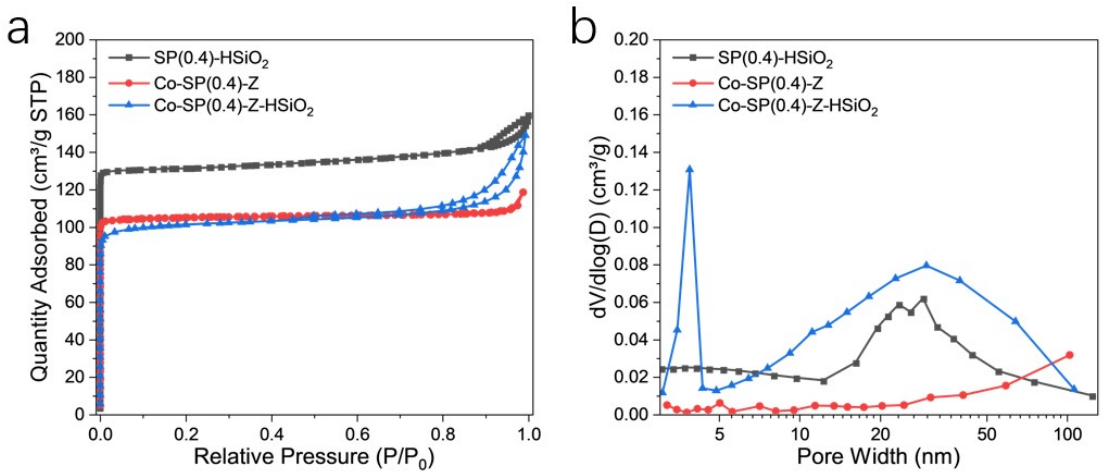

Fig. S11 (a) N_2 adsorption-desorption isotherms and (b) BJH pore size distribution curves of zeolite samples synthesized using hollow SiO_2 and ZIF-67 with different incorporation modes.

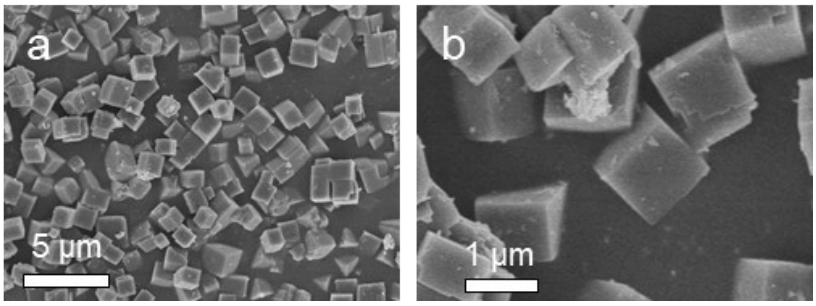

Fig. S12 SEM image of CoSAPO-34 synthesized with a gel composition of Al_2O_3:TEA = 1:4.

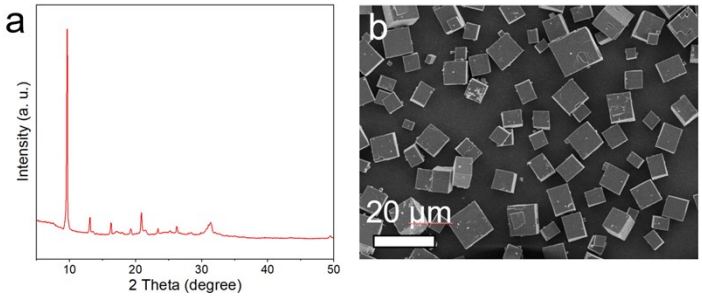

Fig. S13 (a) XRD pattern and (b) SEM image of the hydrothermally synthesized microporous SAPO-34 support.

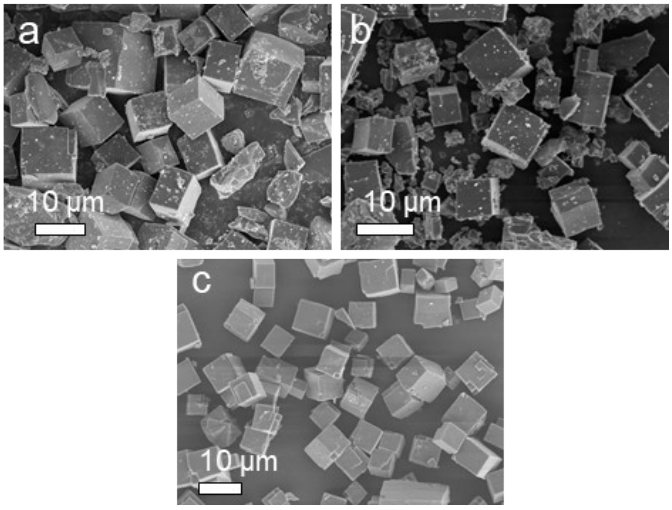

Fig. S14 SEM images of (a) Co/SP-IWI, (b) Co/SP-IE, and (c) Co-SP-IR.

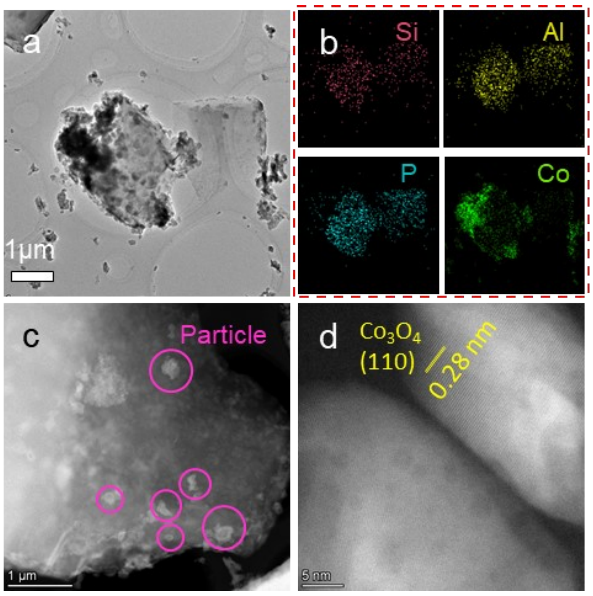

Fig. S15 Structural characterization of Co/SP-IWI: (a) TEM image, (b) EDX elemental mapping, (c) local TEM image, and (d) HR-TEM image.

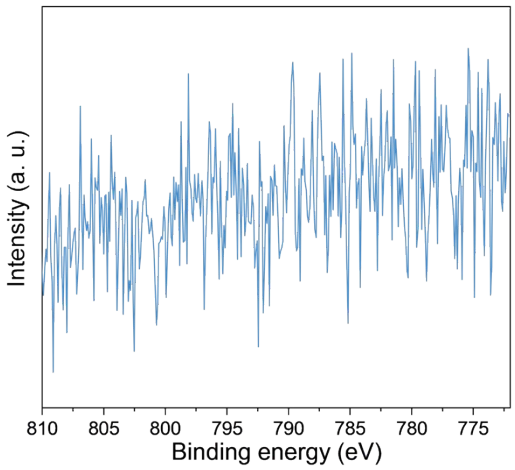

Fig. S16 XPS spectrum of the Co/SP-IE catalyst.

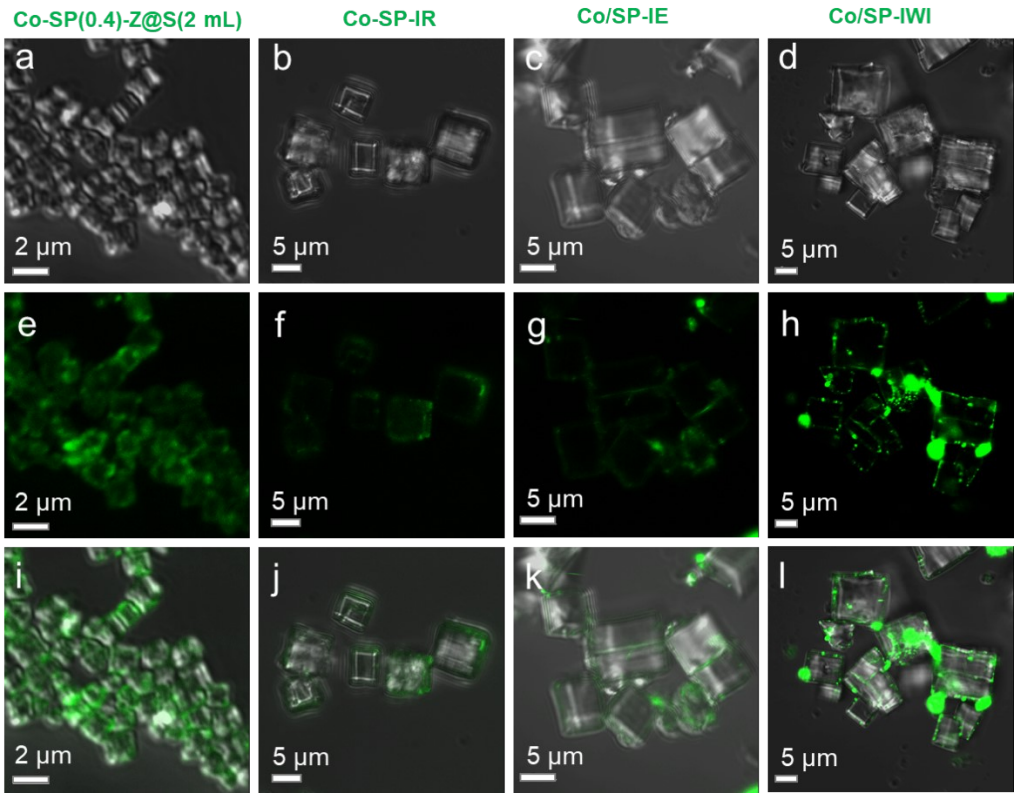

Fig. S17 (a~d) Optical transmission images, (e~h) fluorescence microscopic images and corresponding overlay images of Co-SP(0.4)-Z@S(2mL), Co-SP-IR, Co/SP-IE and Co/SP-IWI.

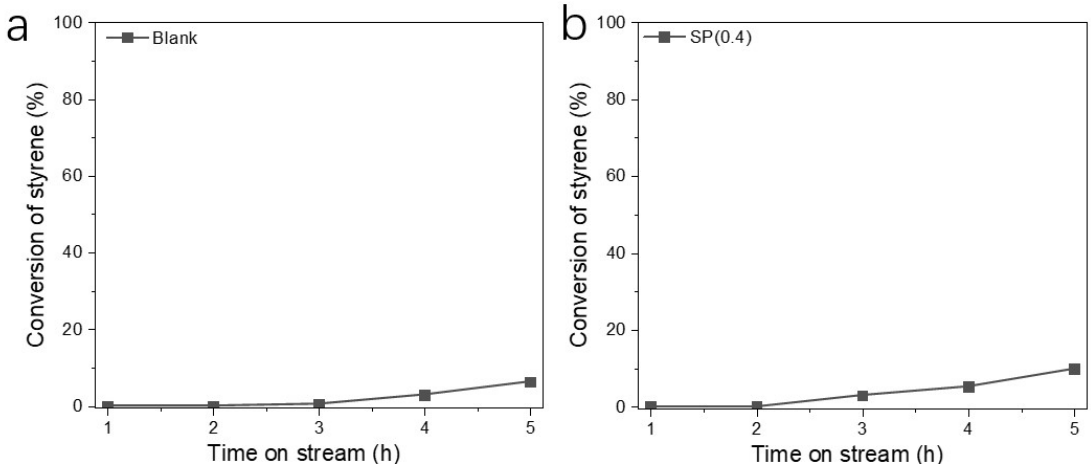

Fig. S18 (a) Blank experiment for the styrene epoxidation reaction without catalyst; (b) Styrene conversion over the metal-free SAPO-34 catalyst.

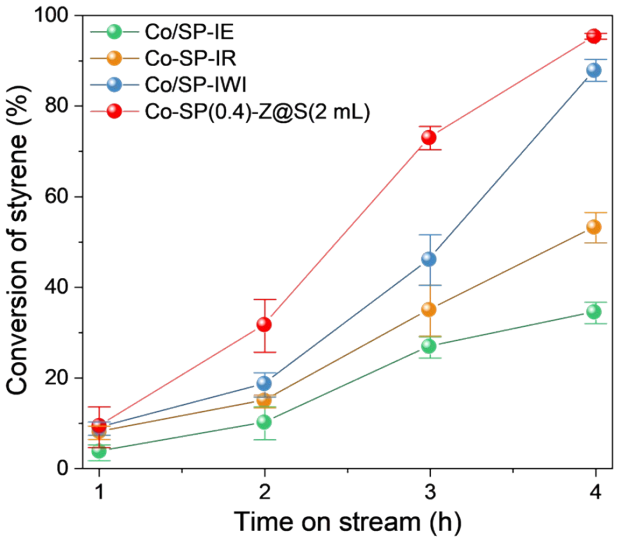

Fig. S19 Conversion of styrene over various catalysts as a function of reaction time.

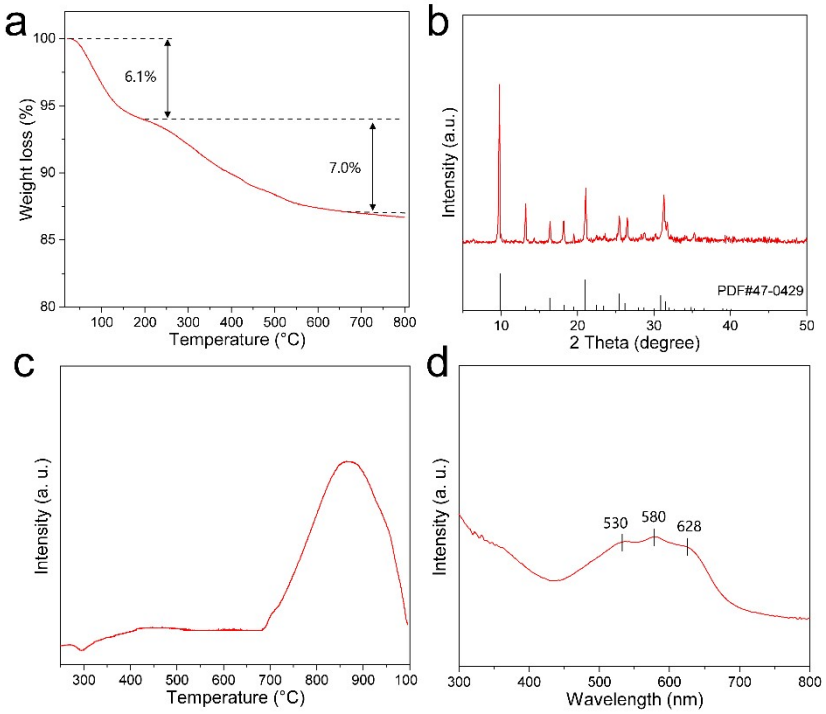

Fig. S20 (a) TG curve of the spent Co-SP(0.4)-Z@S(2mL) catalyst after five cycles; (b) XRD patterns, (c) H_2-TPR profiles, and (d) UV-vis spectra of the regenerated sample after removing carbonaceous species via calcination.

Table S1 Detailed synthesis parameters and gel compositions for the prepared catalysts.

Samples	Precursors				Gel Composition
	Co	Si	Al	P	SiO_2:Al_2O_3:P_2O_5
Co-SP(0.2)-Z@S(4mL)	Z@S(4mL)		pseudo-boehmite	H_3PO_4	0.2:1.0:1.0
Co-SP(0.4)-Z@S(4mL)	Z@S(4mL)		pseudo-boehmite	H_3PO_4	0.4:1.0:1.0
Co-SP(0.6)-Z@S(4mL)	Z@S(4mL)		pseudo-boehmite	H_3PO_4	0.6:1.0:1.0
Co-SP(0.2)-Z@S(2mL)	Z@S(2mL)		pseudo-boehmite	H_3PO_4	0.2:1.0:1.0
Co-SP(0.4)-Z@S(2mL)	Z@S(2mL)		pseudo-boehmite	H_3PO_4	0.4:1.0:1.0
Co-SP(0.6)-Z@S(2mL)	Z@S(2mL)		pseudo-boehmite	H_3PO_4	0.6:1.0:1.0
Co-SP(0.4)-Z	ZIF-67	silica sol	pseudo-boehmite	H_3PO_4	0.4:1.0:1.0
SP(0.4)-$HSiO_2$	-	hollow SiO_2	pseudo-boehmite	H_3PO_4	0.4:1.0:1.0
Co-SP(0.4)-Z-$HSiO_2$	ZIF-67	hollow SiO_2	pseudo-boehmite	H_3PO_4	0.4:1.0:1.0
SP(0.4)	-	silica sol	pseudo-boehmite	H_3PO_4	0.4:1.0:1.0
Co-SP-IR	$Co(NO_3)_2$	silica sol	pseudo-boehmite	H_3PO_4	0.4:1.0:1.0

Table S2 Elemental content of Si and Co in Z@S(2mL) and Z@S(4mL)

Sample	Si (wt.%)	Co (wt.%)
Z@S(2mL)	9.3	19.7
Z@S(4mL)	19.5	14.5

Determined by ICP analysis.

Table S3 Specific surface area and pore structure parameters of the samples derived from N_2 physisorption.

Samples	Surface area (m^2 g^{-1})			Pore volume (cm^3 g^{-1})		
	BET[a]	Micropore[b]	External[c]	Total[d]	Micropore[b]	Mesopore
Co-SP(0.2)-Z@S(4mL)	667	626	41	0.29	0.25	0.04
Co-SP(0.4)-Z@S(4mL)	425	399	26	0.19	0.15	0.04
Co-SP(0.6)-Z@S(4mL)	125	63	32	0.13	0.03	0.10
Co-SP(0.2)-Z@S(2mL)	306	281	26	0.14	0.10	0.04
Co-SP(0.4)-Z@S(2mL)	269	200	69	0.26	0.08	0.18
Co-SP(0.6)-Z@S(2mL)	38	2	36	0.14	0.01	0.13
Co/SP-IWI	504	436	68	0.16	0.25	0.09
Co/SP-IE	425	406	18	0.19	0.16	0.03
Co-SP-IR	466	420	46	0.21	0.15	0.06

a Obtained by BET method,

b Caculated by t-Plot method,

c BET surface area minus micropore surface area

d Volume adsorbed at $P/P_0 = 0.995$.

Note: Due to the inherently non-uniform silicon distribution in SAPO-34 and the occurrence of in-situ growth-etching during the crystallization process, samples with low SiO_2/Al_2O_3 ratios (< 0.2) are particularly susceptible to surface etching, which creates mesoporous structures. As observed in Figure S4a and b, Co-SP(0.2)-Z@S(4mL) exhibits certain etched channels on the crystal surface. Given that the dimensions of these channels are significantly smaller than those of the ZIF-67@SiO_2 template, the contribution of hard-templating to these specific pores can be excluded.Furthermore, owing to the compositional difference, the Si content in Z@S(4mL) is more than double that in Z@S(2mL). This implies that for a targeted Si/Al ratio, the actual mass of hard template added for the Z@S(4mL) series is considerably lower than that for the Z@S(2mL) series. For instance, the mass loading of the template in Co-SP(0.4)-Z@S(4mL) is actually less than that in Co-SP(0.2)-Z@S(2mL). Consequently, although the template dosage was increased according to the Si/Al ratio,

the effective loading in the Z@S(4mL) series remained at a relatively low level. As evidenced by the TEM results of Co-SP(0.6)-Z@S(4mL) (Fig. S5), the use of this thick-shelled template fails to generate distinct internal macropores; instead, it only induces the formation of small crystal aggregates on the external surface, contributing to minor inter-crystalline mesoporosity. Similarly, for Co-SP(0.4)-Z@S(4mL), the low template dosage only results in surface roughening without introducing measurable mesoporosity.

Table S4 Specific surface area and pore volume of zeolite samples derived from different combinations of hollow SiO_2 and ZIF-67.

Samples	Surface area (m^2 g^{-1})			Pore volume (cm^3 g^{-1})		
	BET[a]	Micropore[b]	External[c]	Total[d]	Micropore[b]	Mesopore
SP(0.4)-$HSiO_2$	523	498	25	0.25	0.19	0.06
Co-SP(0.4)-Z	407	397	8	0.18	0.16	0.02
Co-SP(0.4)-Z-$HSiO_2$	388	369	19	0.23	0.15	0.08

a Obtained by BET method,

b Caculated by t-Plot method,

c BET surface area minus micropore surface area

d Volume adsorbed at P/P_0 = 0.995.

Table S5 Cobalt contents of the catalysts determined by ICP-OES.

Sample	Co (wt. %)
Co/SP-IWI	6.1
Co/SP-IE	0.1
Co-SP-IR	5.3
Co-SP(0.4)-Z@S(2mL)	6.2

Table S6 Fitted Parameters of Co K-Edge EXAFS Curves for Co-SP(0.4)-Z@S(2mL) and Co/SP-IWI

Samples (S_0^2=0.744)	path	C.N.[a)]	R (Å) [b)]	σ^2 (10^{-3} Å) [c)]	ΔE (eV) [d)]	R factor [e)]
Co-SP(0.4)-Z@S(2mL)	Co-O	4.2±0.6	2.07±0.02	5.6±3.5	0.28±1.34	0.017
Co/SP-IWI	Co-O	4.8±0.1	1.91±0.01	6.9±1.0	-0.89±1.36	0.012
	Co-Co	2.2±0.3	2.83±0.01	3.1±0.1		
	Co-Co	7.4±2.2	3.34±0.01	9.2±2.7		

a CN is the coordination number;

b R is interatomic distance (the bond length between central atoms and surrounding coordination atoms);

c σ^2 is Debye-Waller factor (a measure of thermal and static disorder in absorber-scatterer distances);

d ΔE_0 is edge-energy shift (the difference between the zero kinetic energy value of the sample and that of the theoretical model).

e R factor is used to value the goodness of the fitting.

Table S7 Catalytic performance data of the catalysts[a].

Sample	Conversion (%)	Reaction rate[b] ($\times 10^{-3}$mol g^{-1} h^{-1})	Selectivity (%)			Yield (%)
			Benzal dehyde	Phenylacetal dehyde	Styrene oxide	
Co/SP-IE	32.1	1.50	20.5	12.9	66.6	21.4
Co-SP-IR	54.5	2.21	23.3	9.9	66.8	36.4
Co/SP-IWI	87.4	2.77	23.8	15.1	61.1	53.4
Co-SP(0.4)-Z@S(2mL)	95.8	4.73	12.6	17.4	70.0	67.1

a. Conditions: 50 mg catalyst, 1.5 mmol styrene in 5 mL DMF, 90 ℃, 40 mL/min air, 4 h.

b. Calculated based on the styrene conversion data at 2 h as shown in **Fig. S19**.

Table S8 Comparison of catalytic performance with previously reported catalysts.

Entry	Catalyst	Oxidant	Styrene (mmol)	Catalyst (mg)	Reaction time (h)	T (°C)	Conv. (%)	Sel. (%)	Yield (%)	Refs
1	Co-SP(0.4)-Z@S(2mL)	Air	1.5	50	4	90	95.8	70.0	67.1	This Work
2	$Cu_{1/2}Co_{1/2}$-MOF-74	Air	0.2	30	48	95	97.6	87.6	85.5	[1]
3	Co^{2+}–NaY(6.2)	O_2	10	200	4	100	45.0	62.0	27.9	[2]
4	Co^{2+}–NaL	O_2	10	200	4	100	18.0	54.0	9.7	[2]
5	Co^{2+}–mordenite	O_2	10	200	4	100	16.0	52.0	8.3	[2]
6	Co^{2+}–beta	O_2	10	200	4	100	26	48	12.5	[2]
7	Fe1/N-doped carbon	O_2	0.44	10	3	140	64.0	89.0	57.0	[3]
8	Hydrotalcite-cys-Au	O_2	-	-	96	80	94	69	64.9	[4]
9	Au/PEG6000-VIC	O_2	3	40	8	100	32.9	72.0	23.7	[5]
10	BaCo-zeolite X	O_2	10	200	4	100	95	83	78.9	[6]
11	N-doped graphene	O_2	8.7	5	10	120	58	40	23.2	[7]
12	Fe-Salen-SBA	Air	10	50	8	80	80.9	59.7	48.3	[8]
13	Co-Salen-SBA	Air	10	50	8	80	49.2	72.4	35.6	[8]
14	NaCo-zeolite X	Air	10	200	4	100	99.0	66.0	65.3	[9]
15	SrCo-zeolite X	Air	10	200	4	100	100	85	85	[9]
16	Co-SAPO-5	Air	3	75	5	90	74.6	70.3	52.4	[10]
17	MOP-Am2	TBHP	0.87	9.1	8	85	60	36	22	[11]
18	CuO@rGO-PC	TBHP	2	97.5	4	70	64.4	50.9	33	[12]
19	Co/IPD-mesoTS-1-5	TBHP	8.7	400	10	100	95.1	52.5	49.9	[13]

REFERENCES

1 H. Liu, W. Liu, G. Xue, T. Tan, C. Yang, P. An, W. Chen, W. Zhao, T. Fan, C. Cui, Z. Tang and G. Li, *J. Am. Chem. Soc.*, 2023, **145**, 11085–11096.

2 Q. Tang, Q. Zhang, H. Wu and Y. Wang, *J. Catal.*, 2005, **230**, 384–397.

3 Y. Xiong, W. Sun, P. Xin, W. Chen, X. Zheng, W. Yan, L. Zheng, J. Dong, J. Zhang, D. Wang and Y. Li, *Adv. Mater.*, 2020, **32**, 2000896.

4 S. R. Leandro, A. C. Mourato, U. Łapińska, O. C. Monteiro, C. I. Fernandes, P. D. Vaz and C. D. Nunes, *J. Catal.*, 2018, **358**, 187–198.

5 A. Zeng, Y. Li, S. Su, D. Li, B. Hou and N. Yu, *J. Catal.*, 2014, **319**, 163–173.

6 X. Yang, Z. Liu, B. Gao, Z. Chen, K. Yan, S. Wang, Y. Xia, Y. Zhang, L. Wang, X. Xu and Y. Tang, *ACS Catal.*, 2023, **13**, 15572–15580.

7 A. Dhakshinamoorthy, A. Primo, P. Concepcion, M. Alvaro and H. Garcia, *Chem. – Eur. J.*, 2013, **19**, 7547–7554.

8 Y. Yang, Y. Zhang, S. Hao and Q. Kan, *Chem. Eng. J.*, 2011, **171**, 1356–1366.

9 J. Sebastian, K. Jinka and R. Jasra, *J. Catal.*, 2006, **244**, 208–218.

10 X.-L. Wei, X.-H. Lu, T.-J. Zhang, X. Chu, D. Zhou, R.-F. Nie and Q.-H. Xia, *Microporous Mesoporous Mater.*, 2015, **214**, 80–87.

11 D. Pathak, R. Khatioda, H. Sharma, A. K. Guha, L. Saikia and B. Sarma, *ACS Appl. Mater. Interfaces*, 2021, **13**, 15353–15365.

12 B. Du, L. Qiu, Y. Chen and Z. Zhang, *ACS Omega*, 2021, **6**, 18157–18168.

13 Y. Shi, L. Chen, J. Li, Q. Hu, G. Ji, Y. Lu, X. Hu, B. Zhu and W. Huang, *Chem. Phys. Lett.*, 2021, **762**, 138116.